Heavy Metal Adsorption Properties and Characterization of Watermelon Peels

*Ndukwu, D.E
Department of Chemistry, Federal College of Education (Technical),
Omoku, Rivers State, Nigeria

Ogukwe, C.E.; Akalezi, C.O; Chukwueke, K.A
Department of Chemistry, Federal University of Technology,
Owerri (FUTO), Nigeria

Didacus, D.E
Department of Petroleum and Gas Engineering, Nigeria Maritime
University, Delta State, Nigeria

Enenebeaku, C.K

*Corresponding author

Abstract
Fruit-processing residues represent a largely underutilized class of agricultural waste with considerable potential for low-cost water treatment applications. This study investigated the capacity of dried watermelon peel (*Citrullus lanatus*) — designated WMP — to adsorb Pb(II), Zn(II), Cu(II), Cr(VI), and Ni(II) ions from synthetic aqueous solutions through systematic batch experimentation. The effects of contact time (30–180 min), adsorbent dose (1–5 g), initial metal concentration (10–90 mg/L), solution pH (2–10), and temperature (30–70°C) were each evaluated. Optimal removal of cationic metals occurred at pH 6, while Cr(VI) showed maximum uptake at pH 4 rather than the strongly acidic pH 2 commonly reported for lignocellulosic adsorbents, peaking at 67% removal — a divergence attributed to the pectin-rich surface chemistry of watermelon peel. Nickel achieved the highest overall removal of 97.0% at 180 minutes, and lead maintained an exceptional 90% efficiency across the entire tested concentration range of 10–50 mg/L. Equilibrium data for Pb^{2+}, Zn^{2+}, Cu^{2+}, and Ni^{2+} conformed best to the Langmuir isotherm (R^2 = 0.972–0.991), while Cr(VI) data fitted the Freundlich model more closely (R^2 = 0.939), indicating a mechanistic divergence in chromium uptake relative to the four cationic metals. The Pseudo-Second-Order kinetic model provided an excellent description of adsorption rates for all five metals (R^2 = 0.998–0.999), implicating chemisorption as the dominant rate-controlling mechanism. Thermodynamic analysis yielded negative $\Delta G°$ values (−0.400 to −0.610 kJ/mol), negative $\Delta H°$, and positive $\Delta S°$ across all systems, confirming spontaneous, mildly exothermic, and entropy-driven adsorption. Scanning electron micrographs revealed a porous, spongy pre-adsorption surface that became densely packed after metal loading, while FTIR spectroscopy identified carboxylate, amine, sulfate, and ester functional groups as binding sites, with pronounced post-adsorption spectral shifts in the carboxylate region confirming the involvement of pectin-derived carboxyl groups in metal complexation. The findings collectively establish WMP as a high-performing, mechanistically distinctive, and eco-friendly biosorbent suitable for multi-metal wastewater treatment.

Keywords: Biosorption; Watermelon Peel; Heavy Metall; Isotherms; Pseudo-Second-Order Kinetics; Thermodynamics; Agricultural Waste; Valorization

Introduction

Contamination of freshwater resources with heavy metals continues to rank among the most pressing environmental challenges globally, driven largely by the unrestricted discharge of industrial effluents from mining, electroplating, battery manufacturing, leather tanning, and metal-processing operations (Mitra et al., 2022). Unlike organic pollutants, heavy metals resist biological degradation, accumulate progressively in sediments and living tissue, and remain toxic at trace concentrations — a combination of properties that makes their removal from water streams a priority concern for environmental regulators worldwide (Bilal et al., 2022).

Lead and chromium are among the most hazardous of the group: lead exposure disrupts neurological development in children and causes renal and cardiovascular damage in adults, while hexavalent chromium is classified as a Group 1 human carcinogen with confirmed mutagenic activity (Balali-Mood et al., 2021). Nickel sensitization is one of the most widespread occupational health risks and contributes to respiratory and dermatological disease; copper and zinc, despite being biologically essential at low concentrations, are acutely toxic at elevated exposure levels (Genchi et al., 2023). These toxicological profiles show the strict discharge limits set by the World Health Organization, which compel industries to adopt effective and financially viable treatment approaches (WHO, 2022).

Conventional remediation technologies — including chemical precipitation, ion exchange, electrocoagulation, membrane filtration, and advanced oxidation — achieve high removal efficiencies but impose prohibitive costs in terms of chemical reagent consumption, energy requirements, and secondary sludge disposal, particularly when applied at small- to medium-industrial scale (Vunain et al., 2023). Adsorption using low-cost biosorbents derived from agricultural residues has consequently gained considerable traction as a complementary strategy, offering flexibility of design, simple operation, and the possibility of diverting waste streams away from open dumping or burning (Raji et al., 2023).

Watermelon (*Citrullus lanatus*) is one of the world's most widely cultivated fruits, with global production exceeding 100 million tonnes annually, generating enormous quantities of peel waste that is typically discarded without commercial recovery (Mathew et al., 2023). Watermelon peel is compositionally distinct from most lignocellulosic agro-residues in that it contains a significant proportion of pectin — a highly branched polysaccharide whose galacturonic acid backbone is rich in carboxyl groups — alongside cellulose, hemicellulose, and small quantities of lignin (Anastopoulos et al., 2022). This pectin-derived carboxylate density makes watermelon peel chemically well-suited to coordinate divalent metal cations through electrostatic attraction and surface complexation, and potentially provides a distinct sorption environment for anionic chromate species as well.

Although several studies have explored watermelon peel for single-metal adsorption, comprehensive multi-parameter investigations covering five metals simultaneously, alongside full isotherm, kinetic, thermodynamic, and spectroscopic characterization, remain comparatively scarce in the literature. This study addresses that gap through a systematic batch evaluation of WMP for the concurrent removal of Pb(II), Zn(II), Cu(II), Cr(VI), and Ni(II), with detailed interpretation of the results. The findings contribute both to the scientific understanding of pectin-rich biosorbents and to the practical case for watermelon peel as a valuable, zero-cost raw material for multi-metal water remediation.

Materials and Methods

Biosorbent Collection and Preparation

Fresh watermelon peels (*Citrullus lanatus*) were obtained from local fruit vendors in Omoku, Rivers State, Nigeria. The peels were thoroughly washed under running tap water to remove residual pulp and surface contaminants, rinsed with deionized water, and cut into small pieces for drying. After preliminary air-drying, the material was transferred to a thermostated oven maintained at 60°C until a constant weight was achieved. The dried peels were pulverized using a pulveriser and passed through a 300 μm mechanical sieve to obtain uniform-sized particles. The resulting WMP powder was stored in sealed polyethylene bags until required for experiments.

Preparation of Metal Ion Solutions

Stock solutions of 1000 mg/L were prepared for each target metal ion from analytical-grade salts: lead(II) chloride ($PbCl_2$), copper(II) tetraoxosulphate(VI) pentahydrate ($CuSO_4 \cdot 5H_2O$), zinc(II) chloride ($ZnCl_2$), nickel(II) chloride hexahydrate ($NiCl_2 \cdot 6H_2O$), and potassium dichromate ($K_2Cr_2O_7$),

dissolved in measured volumes of deionized water in 1-litre volumetric flasks. Working solutions at concentrations of 10, 30, 50, 70, and 90 mg/L were prepared by serial dilution of the respective stock solutions. All reagents were of analytical reagent grade.

Batch Adsorption Procedure

In each batch experiment, 1 g of WMP powder was contacted with 100 mL of metal ion solution in 250-mL conical flasks, agitated at 200 rpm on an orbital shaker. At specified intervals, aliquots were withdrawn, filtered through Whatman 0.45 μm membrane filters, and the filtrate analyzed for residual metal concentration using an Atomic Absorption Spectrophotometer (AAS). The percentage removal (R%) and equilibrium adsorption capacity (qe, mg/g) were calculated as:

$$R\% = [(C_0 - Ce) / C_0] \times 100$$
$$qe = [(C_0 - Ce) \times V] / m$$

where C_0 and Ce are the initial and equilibrium concentrations (mg/L), V is the solution volume (L), and m is the adsorbent mass (g). Parameters investigated were: contact time (30–180 min), adsorbent dose (1–5 g per 100 mL), initial metal concentration (10–90 mg/L), solution pH (2–10, adjusted using 0.1 M HCl or 0.1 M NaOH measured with a calibrated pH meter), and solution temperature (30–70°C, regulated via a thermostated water bath).

Adsorption Isotherm Models

Equilibrium data were fitted to the linearized Langmuir and Freundlich isotherm models. The Langmuir model is expressed as:

$$Ce/qe = 1/(qm \cdot KL) + Ce/qm$$

where qm (mg/g) is the theoretical maximum monolayer adsorption capacity and KL (L/mg) is the Langmuir affinity constant. The Freundlich model is given by:

$$\log qe = \log KF + (1/n) \log Ce$$

where KF is the Freundlich capacity factor and 1/n is the heterogeneity index; values of 1/n below unity typically indicate favourable adsorption (Foo & Hameed, 2010).

Kinetic Models

The Pseudo-First-Order (PFO) model of Lagergren (1898) and the Pseudo-Second-Order (PSO) model of Ho and McKay (1999) were applied to time-dependent uptake data:

$$PFO: \log(qe - qt) = \log qe - (k_1/2.303)t$$
$$PSO: t/qt = 1/(k_2 qe^2) + t/qe$$

The best-fitting model was selected based on the coefficient of determination (R^2) and the agreement between calculated (qe,cal) and experimental (qe,exp) equilibrium capacities.

Thermodynamic Analysis

Thermodynamic parameters were derived from the temperature dependence of the distribution coefficient Kc (= qe/Ce) using the van't Hoff equation:

$$\ln Kc = \Delta S°/R - \Delta H°/RT; \quad \Delta G° = -RT \ln Kc$$

where R = 8.314 J/mol·K and T is the absolute temperature in Kelvin. The slope and intercept of the plot of ln Kc versus 1/T yielded ΔH° and ΔS°, respectively (Tran et al., 2021).

Biosorbent Characterization

Surface morphology of WMP before and after metal adsorption was examined using Scanning Electron Microscopy (SEM) at 2000× magnification. Fourier Transform Infrared (FTIR) spectroscopy was employed to identify surface functional groups and observe spectral shifts resulting from metal binding, scanning across the wavenumber range of 400–4000 cm^{-1}.

Results and Discussion

Optimal Batch Adsorption Conditions

Preliminary batch screening identified the optimal contact time, dose, initial concentration, pH, and temperature for each metal–WMP system. The results are summarized in Table 1.

Table 1. Optimal batch adsorption conditions for heavy metal removal by WMP

Metal Ion	Optimum Time (min)	Dose (g)	Init. Conc. (mg/L)	pH	Temp (°C)
Pb^{2+}	60	3	50	6	40
Zn^{2+}	60	2	50	6	40
Cu^{2+}	60	2	50	6	40
Cr	30	2	30	4	30
Ni^{2+}	60	2	30	6	40

A critical observation from Table 1 is the contrasting pH requirements across the five metal systems. While the four cationic metals — Pb^{2+}, Zn^{2+}, Cu^{2+}, and Ni^{2+} — all performed best at pH 6, the optimal pH for Cr removal was pH 4. This is notably different from the pH 2 optimum typically observed for chromate adsorption on woody or leafy lignocellulosic biosorbents and reflects the distinct surface acidity of the pectin-rich WMP matrix. The presence of pectin galacturonate groups, which protonate over a slightly wider acid range than purely cellulosic surfaces, may create an optimum electrostatic environment for chromate anion capture at the moderately acidic pH 4 (Shehu & Ibrahim, 2023). The shorter equilibrium time recorded for Cr (30 min) relative to the cationic metals (60 min), and the lower initial concentration used for Cr and Ni (30 mg/L versus 50 mg/L for Pb, Zn, and Cu), further reflect the mechanistic distinctions between anionic and cationic metal uptake on this biosorbent.

Effect of Contact Time

The influence of contact time on metal uptake by WMP was examined over 30–180 minutes. Results are presented in Table 2 and illustrated in Figure 1.

Table 2. Effect of contact time on heavy metal adsorption onto WMP

Metal	Time (min)	Vol (L)	C_o (mg/L)	Ce (mg/L)	qe (mg/g)	% Removal
Pb^{2+}	30	0.107	50	18.0	1.19	64.0
	60	0.105	50	10.0	1.43	80.0
	90	0.108	50	4.5	1.54	91.0
	120	0.104	50	4.0	1.48	92.0
	150	0.106	50	3.5	1.53	93.0
	180	0.103	50	3.2	1.58	93.6

Zn^{2+}	30	0.103	50	20.0	1.55	60.0
	60	0.106	50	16.0	1.79	68.0
	90	0.101	50	14.0	1.86	72.0
	120	0.107	50	12.0	1.94	76.0
	150	0.105	50	10.0	2.00	80.0
	180	0.108	50	8.5	2.10	83.0
Cu^{2+}	30	0.108	50	16.0	1.70	68.0
	60	0.105	50	7.0	2.05	86.0
	90	0.107	50	5.5	2.13	89.0
	120	0.104	50	4.5	2.23	91.0
	150	0.106	50	3.5	2.34	93.0
	180	0.102	50	3.0	2.40	94.0
Cr	30	0.102	30	4.5	1.31	85.0
	60	0.104	30	3.6	1.36	88.0
	90	0.108	30	3.0	1.40	90.0
	120	0.105	30	2.4	1.44	92.0
	150	0.107	30	1.9	1.47	93.7
	180	0.103	30	1.6	1.51	94.7
Ni^{2+}	30	0.106	30	2.7	1.42	91.0
	60	0.108	30	2.1	1.47	93.0
	90	0.104	30	1.6	1.53	94.7
	120	0.107	30	1.3	1.54	95.7
	150	0.105	30	1.0	1.59	96.7
	180	0.101	30	0.9	1.63	97.0

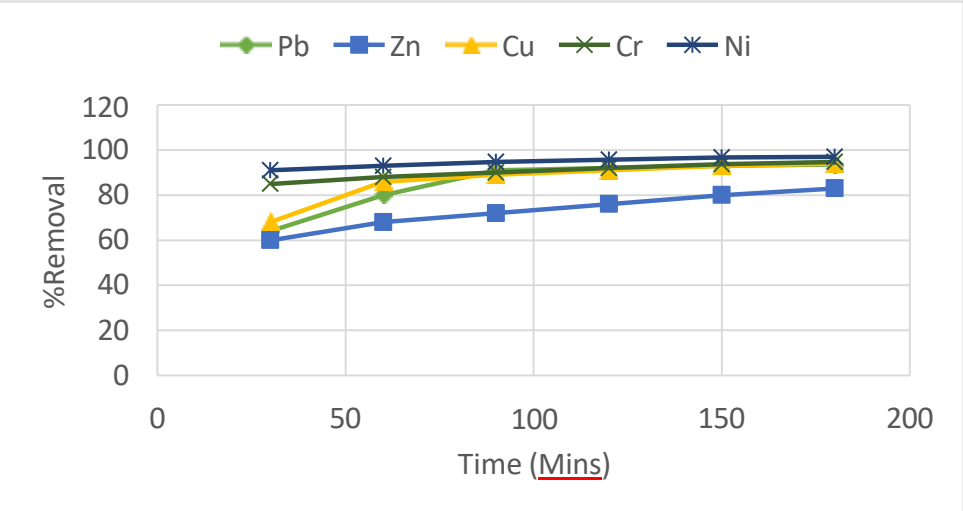

Figure 1. Effect of contact time on the percentage removal of Pb^{2+}, Zn^{2+}, Cu^{2+} , Cr , and Ni^{2+} onto WMP.

A two-phase kinetic pattern was consistently observed across all five metal systems: a rapid initial uptake phase driven by the abundance of unoccupied active sites on the WMP surface, followed by a progressively slower approach to equilibrium as site availability diminishes and the residual concentration gradient weakens (Raji et al., 2023). Lead removal rose sharply from 64% at 30 minutes to 91% at 90 minutes, increasing only marginally thereafter to reach 93.6% at 180 minutes. This pattern indicates that effective equilibrium for Pb^{2+} is approached within the first 90 minutes, with subsequent increments offering diminishing practical returns.

Zinc showed the slowest approach to equilibrium among the five metals, rising steadily from 60% at 30 minutes to 83% at 180 minutes without a clear plateau, suggesting that Zn^{2+} diffusion into the internal pore structure of the WMP matrix is comparatively rate-limiting relative to the surface-controlled uptake seen for other cations (Onyancha et al., 2024). Copper displayed an efficient two-stage profile: a rapid climb from 68% to 86% between 30 and 60 minutes, followed by a slower increase to 94% by 180 minutes, consistent with fast occupation of readily accessible carboxylate sites on the peel surface followed by slower intraparticle migration.

Particularly impressive performances were recorded for Cr and Ni^{2+}. Chromium removal from the 30 mg/L solution reached 85% within just 30 minutes and climbed steadily to 94.7% at 180 minutes, indicating strong and rapid electrostatic attraction between protonated WMP surface groups and chromate anions at the applied pH of 4. Nickel achieved the highest removal of all five metals, reaching 91% at the first measurement point of 30 minutes and increasing to an exceptional 97.0% at 180 minutes — a performance that underlines the particularly high affinity of WMP's carboxyl and amine groups for Ni^{2+} ions under near-neutral pH conditions. On the basis of these profiles, 90 minutes was selected as the working equilibrium time for Pb^{2+}, Zn^{2+}, and Cu^{2+}, and 30 minutes for Cr and Ni^{2+}, consistent with the optimal conditions in Table 1.

Effect of Adsorbent Dose

The adsorbent dose was varied from 1 g to 5 g per 100 mL of solution to evaluate its influence on both removal efficiency and adsorption capacity. Results are presented in Table 3.

Table 3. Effect of adsorbent dose on heavy metal adsorption onto WMP

Metal	Dose (g)	Vol (L)	C_0 (mg/L)	Ce (mg/L)	qe (mg/g)	% Removal
Pb^{2+}	1.0	0.107	50	17.0	3.53	66.0
	2.0	0.105	50	10.0	2.10	80.0
	3.0	0.108	50	4.5	1.54	91.0
	4.0	0.104	50	3.0	1.22	94.0
	5.0	0.106	50	2.0	1.13	96.0
Zn^{2+}	1.0	0.103	50	25.0	2.67	50.0
	2.0	0.106	50	16.0	1.79	68.0
	3.0	0.101	50	12.0	1.31	76.0
	4.0	0.107	50	9.0	1.10	82.0
	5.0	0.105	50	7.0	0.92	86.0
Cu^{2+}	1.0	0.108	50	18.0	3.33	64.0
	2.0	0.105	50	7.0	2.05	86.0

	3.0	0.107	50	5.0	1.50	90.0
	4.0	0.104	50	3.5	1.21	93.0
	5.0	0.106	50	2.5	1.12	95.0
Cr	1.0	0.102	30	15.0	1.57	50.0
	2.0	0.104	30	9.9	1.04	67.0
	3.0	0.108	30	7.0	0.89	76.7
	4.0	0.105	30	5.0	0.66	83.3
	5.0	0.107	30	3.5	0.53	88.3
Ni^{2+}	1.0	0.106	30	12.0	1.81	60.0
	2.0	0.108	30	9.0	1.16	70.0
	3.0	0.104	30	7.0	0.96	76.7
	4.0	0.107	30	5.0	0.70	83.3
	5.0	0.105	30	3.5	0.56	88.3

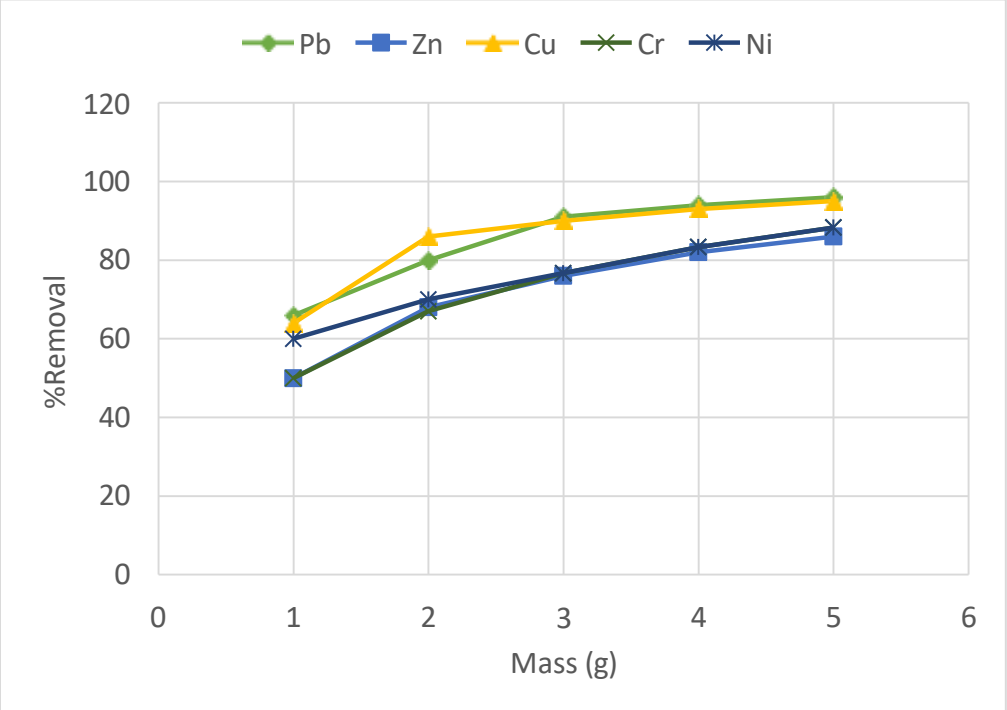

Figure 2. Effect of adsorbent dose on the percentage removal of Pb^{2+}, Zn^{2+}, Cu^{2+}, Cr , and Ni^{2+} onto WMP.

For all five metals, percentage removal increased with rising dose while the equilibrium adsorption capacity (qe) declined, a well-documented inverse relationship arising from the growing number of available binding sites at higher adsorbent loadings, offset by diminishing utilization of each gram of material as more sites remain unoccupied relative to the fixed metal supply (Murphy et al., 2023). Pb^{2+} removal climbed dramatically from 66% at 1 g to 91% at just 3 g — the selected optimum — before continuing to 96% at 5 g. The sharp efficiency gains between 1 g and 3 g indicate that this metal finds abundant and readily accessible binding sites on the WMP surface, while the qe decline

from 3.53 to 1.54 mg/g over the same range reflects the partial utilization of the additional sites introduced by higher doses.

Copper removal followed a closely comparable trajectory, rising from 64% at 1 g to 90% at 3 g and reaching 95% at maximum dose, with qe dropping from 3.33 to 1.50 mg/g — reflecting the strong affinity of pectin carboxylate groups for Cu^{2+}, which ensures efficient occupation of surface sites even at lower doses. Zinc and nickel produced more gradual dose-response curves, with Zn^{2+} increasing from 50% at 1 g to a maximum of 86% at 5 g, and Ni^{2+} climbing from 60% to 88.3% over the same range. The selected 2 g optimum for both Zn^{2+} and Ni^{2+} represents the point of reasonable efficiency before strongly diminishing returns in qe set in. For Cr, 2 g yielded 67% removal from the 30 mg/L solution, with qe declining from 1.57 mg/g at 1 g to 0.53 mg/g at 5 g. The dose-response plateau being reached earlier for Cr than for the cationic metals suggests that the density of positively charged surface groups under acidic conditions, rather than total surface area, limits chromate uptake beyond a certain dose (Akhtar et al., 2024).

Effect of Initial Metal Ion Concentration

The effect of initial concentration on adsorption performance was investigated across a range of 10–90 mg/L for Pb^{2+}, Zn^{2+}, Cu^{2+}, and Ni^{2+}, and 10–90 mg/L for Cr. Results are presented in Table 4.

Table 4. Effect of initial metal concentration on adsorption onto WMP

Metal	C_0 (mg/L)	Vol (L)	Ce (mg/L)	qe (mg/g)	% Removal
Pb^{2+}	10	0.107	1.0	0.33	90.0
	30	0.105	3.0	0.90	90.0
	50	0.108	5.0	1.39	90.0
	70	0.104	10.0	1.85	85.7
	90	0.106	16.0	2.26	82.2
Zn^{2+}	10	0.103	2.0	0.41	80.0
	30	0.106	6.0	1.27	80.0
	50	0.101	16.0	1.79	68.0
	70	0.107	28.0	2.20	60.0
	90	0.105	42.0	2.40	53.3
Cu^{2+}	10	0.108	1.5	0.46	85.0
	30	0.105	4.5	1.36	85.0
	50	0.107	13.5	1.95	73.0
	70	0.104	22.0	2.50	68.6
	90	0.106	32.0	2.92	64.4
Cr	10	0.102	3.8	0.32	62.0
	30	0.104	9.9	1.04	67.0
	50	0.108	20.0	1.39	60.0
	70	0.105	32.0	1.81	54.3

	90	0.107	45.0	2.10	50.0
Ni^{2+}	10	0.106	2.0	0.42	80.0
	30	0.108	6.0	1.33	80.0
	50	0.104	17.0	1.73	66.0
	70	0.107	28.0	2.24	60.0
	90	0.105	40.0	2.62	55.6

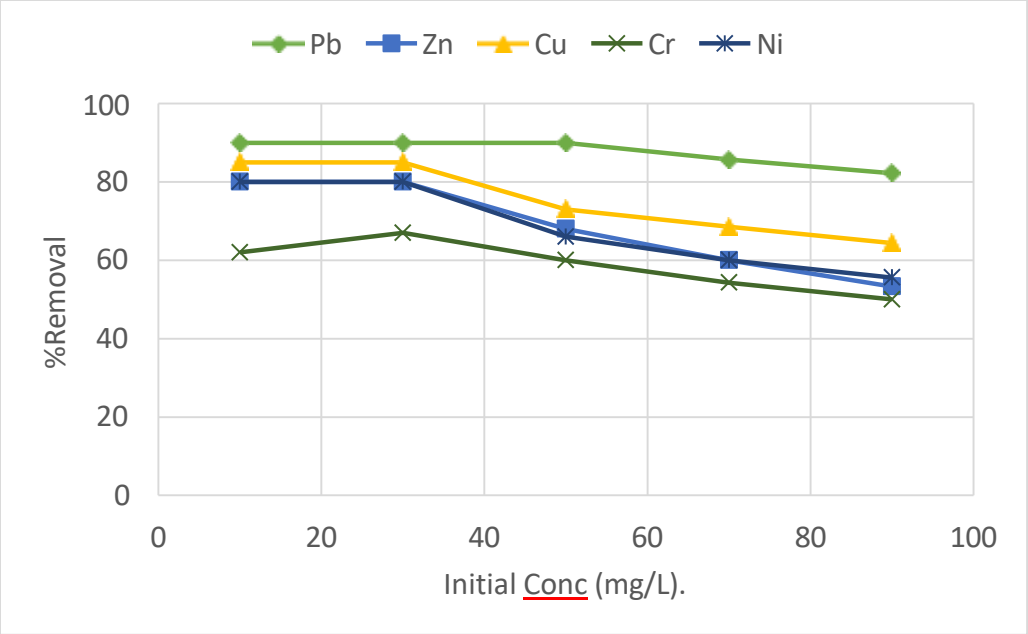

Figure 3. Effect of initial metal concentration on percentage removal by WMP for Pb^{2+}, Zn^{2+}, Cu^{2+}, Cr, and Ni^{2+}.

Lead showed an exceptional concentration-stability profile: removal remained constant at 90% across the entire 10–50 mg/L range before declining to 85.7% at 70 mg/L and 82.2% at 90 mg/L. This high and sustained efficiency across a wide loading range suggests that the WMP surface provides sufficient high-affinity sites to bind Pb^{2+} without significant competition until concentrations well above 50 mg/L, a behavior characteristic of adsorbents with strong metal-selective functional groups (Anastopoulos et al., 2022). Nickel similarly maintained 80% removal up to 30 mg/L before declining more steeply to 55.6% at 90 mg/L, while copper held 85% efficiency for concentrations up to 30 mg/L before exhibiting a more pronounced decline to 64.4% at the highest loading tested.

Zinc and chromium showed the most concentration-sensitive removal profiles. Zinc fell from 80% at lower loadings to 53.3% at 90 mg/L, consistent with the comparatively shallow dose-response and slower kinetics noted earlier for this metal, suggesting relatively limited high-affinity Zn^{2+} sites on the WMP surface relative to other cations. Chromium removal declined from 62% at 10 mg/L to 50% at 90 mg/L — still a meaningful removal fraction, but reflecting the progressively limited electrostatic capacity of the protonated surface sites available for chromate binding as the anionic loading intensifies (Bashir et al., 2023). The steady increase in qe values across the full concentration range for every metal confirms that the absolute quantity of metal bound per gram of WMP continues rising with concentration, driven by the increasing mass-transfer gradient.

Effect of Solution pH

Solution pH was varied from 2 to 10 to determine its influence on metal uptake by WMP. Results are presented in Table 5.

Table 5. Effect of solution pH on heavy metal adsorption onto WMP

Metal	pH	Vol (L)	C_o (mg/L)	Ce (mg/L)	qe (mg/g)	% Removal
Pb^{2+}	2	0.107	50	43.0	0.37	14.0
	4	0.105	50	24.0	0.91	52.0
	6	0.108	50	15.0	1.26	70.0
	8	0.104	50	17.5	1.12	65.0
	10	0.106	50	21.0	1.02	58.0
Zn^{2+}	2	0.103	50	42.0	0.41	16.0
	4	0.106	50	23.0	1.43	54.0
	6	0.101	50	16.0	1.79	68.0
	8	0.107	50	18.5	1.68	63.0
	10	0.105	50	22.0	1.47	56.0
Cu^{2+}	2	0.108	50	41.0	0.50	18.0
	4	0.105	50	21.0	1.52	58.0
	6	0.107	50	13.5	1.95	73.0
	8	0.104	50	16.0	1.77	68.0
	10	0.106	50	19.5	1.61	61.0
Cr	2	0.102	30	12.0	0.92	60.0
	4	0.104	30	9.9	1.04	67.0
	6	0.108	30	15.0	0.83	50.0
	8	0.105	30	18.0	0.63	40.0
	10	0.107	30	21.0	0.48	30.0
Ni^{2+}	2	0.106	30	25.5	0.24	15.0
	4	0.108	30	14.0	0.86	53.3
	6	0.104	30	9.0	1.12	70.0
	8	0.107	30	11.0	1.02	63.3
	10	0.105	30	13.5	0.87	55.0

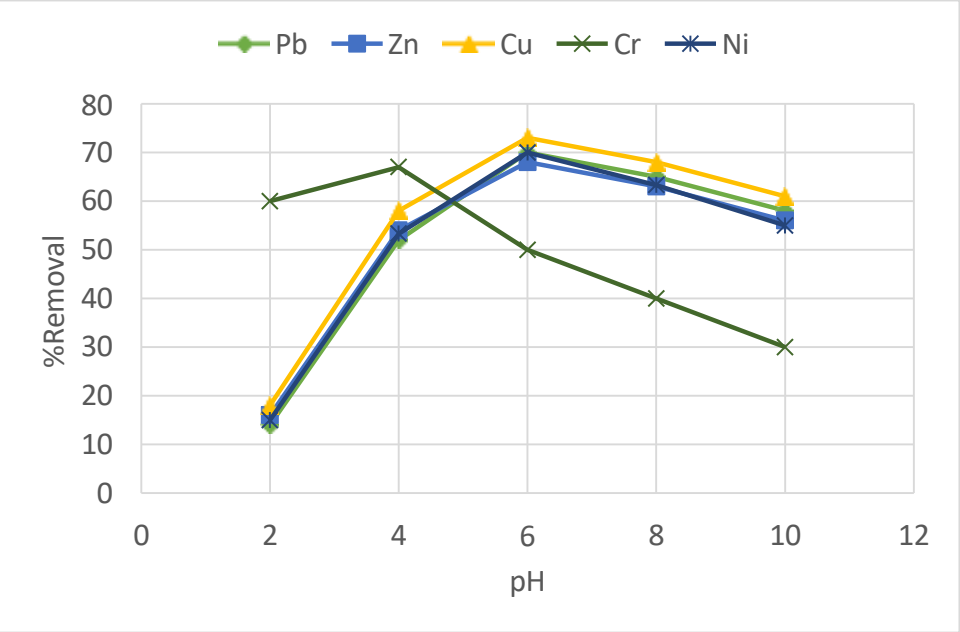

Figure 4. Effect of solution pH on percentage removal by WMP for Pb^{2+}, Zn^{2+}, Cu^{2+}, Cr, and Ni^{2+}.

The four cationic metals all exhibited a characteristic bell-shaped pH profile with optimal removal at pH 6: Cu^{2+} achieved the highest peak removal of 73%, followed by Zn^{2+} (68%), Pb^{2+} (70%), and Ni^{2+} (70%). At strongly acidic conditions (pH 2), removal efficiencies were markedly suppressed — falling to as low as 14% for Pb^{2+} and 15% for Ni^{2+} — because heavy protonation of carboxyl and hydroxyl groups on the WMP surface creates a net positive charge that electrostatically repels cationic metal species, while high H^{+} concentrations compete directly with metal ions for binding sites (Macena et al., 2023). As pH increases toward 6, progressive deprotonation of the pectin galacturonate groups exposes increasing densities of negatively charged carboxylate sites well-suited to coordinate divalent cations through ion exchange and surface complexation. The decline in removal beyond pH 6–8 is consistent with the onset of metal hydroxide precipitation at higher pH and changes in surface speciation of both adsorbent and adsorbate.

The chromium pH profile was notably distinct and mechanistically revealing. Rather than peaking at pH 2 as is typical for chromate adsorption on cellulosic or woody biosorbents, removal on WMP reached its maximum of 67% at pH 4, declining progressively to just 30% at pH 10. The 60% removal even at pH 2 confirms that surface protonation still drives meaningful electrostatic attraction, but the optimum at pH 4 suggests that at this intermediate acidity, the balance between the density of protonated surface sites and the dominant Cr(VI) species in solution ($HCrO_4^-$ predominates between approximately pH 1–6) is most favorable on the pectin surface. This contrasts with the pH 2 optima observed for EGL and COS in parallel experiments and highlights that the composition of the biosorbent surface — particularly the proportion of pectin-derived groups relative to lignin and cellulose — meaningfully shifts the chromate adsorption optimum, a distinction consistent with findings reported by Shehu and Ibrahim (2023) for pectin-bearing fruit waste materials.

Effect of Temperature

The effect of temperature on adsorption was investigated across 30–70°C. Results are presented in Table 6.

Table 6. Effect of temperature on heavy metal adsorption onto WMP

Metal	Temp (°C)	Vol (L)	C_0 (mg/L)	Ce (mg/L)	qe (mg/g)	% Removal
Pb^{2+}	30	0.107	50	3.20	2.45	93.6
	40	0.108	50	3.50	2.45	93.0
	50	0.105	50	4.50	2.48	91.0
	60	0.104	50	4.80	2.44	90.4
	70	0.106	50	6.00	2.47	88.0
Zn^{2+}	30	0.103	50	8.00	2.86	84.0
	40	0.106	50	7.20	2.43	85.6
	50	0.101	50	8.50	2.25	83.0
	60	0.107	50	9.00	2.14	82.0
	70	0.105	50	10.50	2.16	79.0
Cu^{2+}	30	0.108	50	8.50	2.95	83.0
	40	0.105	50	9.00	2.92	82.0
	50	0.107	50	11.00	2.86	78.0
	60	0.104	50	11.50	2.82	77.0
	70	0.106	50	14.00	2.80	72.0
Cr	30	0.102	30	4.80	1.08	84.0
	40	0.104	30	5.00	1.08	83.3
	50	0.108	30	6.00	1.06	80.0
	60	0.105	30	6.20	1.05	79.3
	70	0.107	30	7.50	1.06	75.0
Ni^{2+}	30	0.106	30	2.80	1.54	90.7
	40	0.108	30	3.00	1.52	90.0
	50	0.104	30	3.80	1.53	87.3
	60	0.107	30	4.00	1.50	86.7
	70	0.105	30	5.00	1.53	83.3

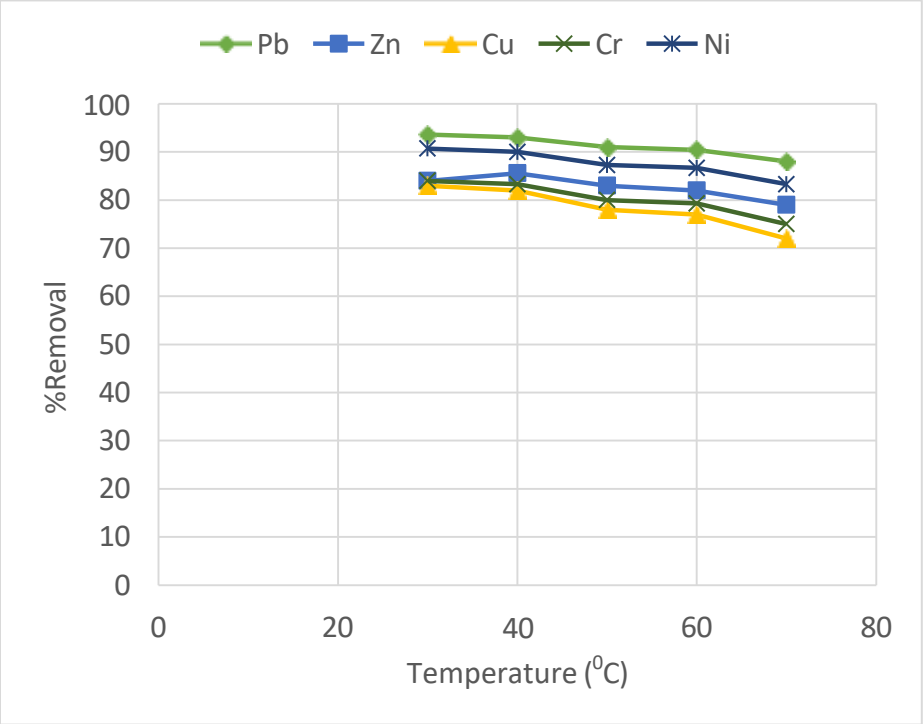

Figure 5. Effect of temperature on percentage removal by WMP for Pb^{2+}, Zn^{2+}, Cu^{2+}, Cr, and Ni^{2+}.

A general decline in percentage removal with increasing temperature was observed for all five metals, indicating that the adsorption processes are exothermic in nature and that higher temperatures thermodynamically favour the reverse desorption step, reducing equilibrium surface loading (Tran et al., 2021). Lead removal started from an impressive 93.6% at 30°C and declined gradually to 88.0% at 70°C, while qe values remained relatively stable between 2.44–2.48 mg/g throughout the temperature range — indicating that, despite the modest efficiency decline, the mass of Pb^{2+} bound per gram of WMP stays nearly constant, reflecting strong binding that resists thermal disruption across the tested range.

Zinc exhibited a slight non-monotonic behavior: removal increased marginally from 84.0% at 30°C to 85.6% at 40°C before declining progressively to 79.0% at 70°C. This minor initial uptick may reflect a small activation energy barrier for Zn^{2+} diffusion into the WMP pore network that is overcome at 40°C, after which the exothermic equilibrium thermodynamics prevail and drive removal downward (Adeyemo et al., 2022). Copper fell from 83% at 30°C to 72% at 70°C, chromium from 84.0% to 75.0%, and nickel from 90.7% to 83.3%. The temperature sensitivity was relatively mild for all metals, which has favorable practical implications: WMP-based treatment systems can operate efficiently at ambient temperatures without heating, avoiding the energy costs associated with thermally driven processes.

Adsorption Isotherm Studies

To understand the distribution of metal ions between the WMP surface and the aqueous phase at equilibrium, experimental data were fitted to the Langmuir and Freundlich isotherm models. Derived parameters and model fits are compiled in Table 7, with the corresponding plots presented as Figures 6 and 7.

Table 7. Langmuir and Freundlich isotherm fitting parameters for heavy metal adsorption onto WMP

Metal	qm (mg/g)	KL (L/mg)	R^2 (L)	KF	1/n	n	R^2 (F)	Best Fit
Pb^{2+}	0.287	-0.403	0.986	4.074	1.391	0.719	0.965	Langmuir
Zn^{2+}	0.333	-0.286	0.991	6.976	1.639	0.609	0.918	Langmuir
Cu^{2+}	0.272	-0.377	0.981	4.440	1.651	0.605	0.946	Langmuir
Cr	0.297	-0.119	0.908	13.948	1.275	0.784	0.939	Freundlich
Ni^{2+}	0.306	-0.272	0.972	6.723	1.620	0.617	0.927	Langmuir

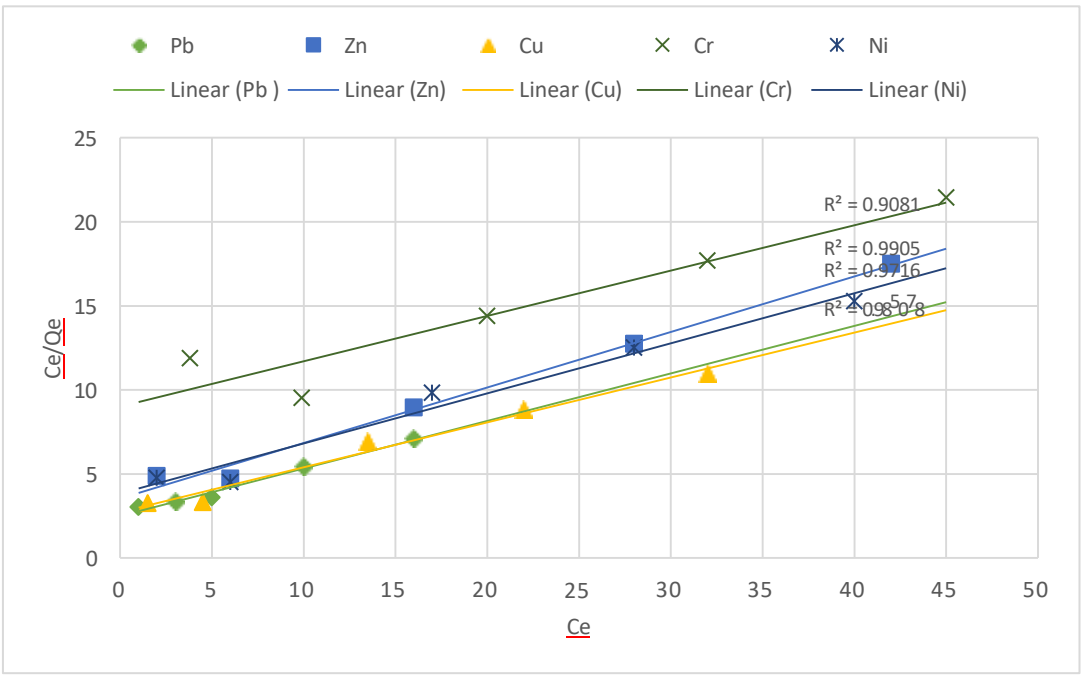

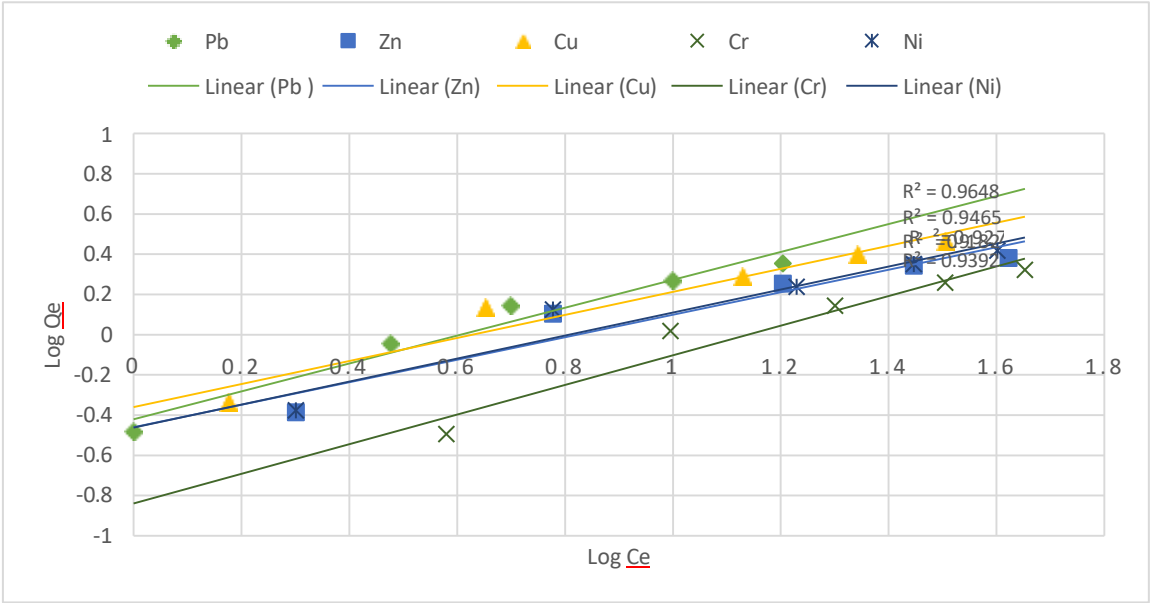

Figures 6 and 7. Langmuir (up) and Freundlich (down) isotherm plots for adsorption of Pb^{2+}, Zn^{2+}, Cu^{2+}, Cr, and Ni^{2+} onto WMP.

The isotherm data for WMP revealed a genuinely mixed pattern that is mechanistically informative. Four metals — Pb^{2+} (R^2 = 0.986), Zn^{2+} (R^2 = 0.991), Cu^{2+} (R^2 = 0.981), and Ni^{2+} (R^2 = 0.972) — were better described by the Langmuir model, suggesting monolayer adsorption on a relatively homogeneous set of energetically equivalent sites. The comparable maximum monolayer capacities (qm) derived for these metals — 0.287 mg/g for Pb^{2+}, 0.333 mg/g for Zn^{2+}, 0.272 mg/g for Cu^{2+}, and 0.306 mg/g for Ni^{2+} — are consistent with the hypothesis that the pectin-derived carboxylate groups on WMP serve as a uniform class of binding site for these divalent cations, producing the near-homogeneous surface behavior described by Langmuir theory (Mathew et al., 2023).

Chromium presented a mechanistically distinct isotherm: its equilibrium data were better described by the Freundlich model (R^2 = 0.939) than by the Langmuir equation (R^2 = 0.908). This divergence — the only metal among the five for which Freundlich outperformed Langmuir on WMP — points to a more heterogeneous, energetically distributed binding environment for chromate anions on the WMP surface, a finding consistent with the proposed involvement of multiple surface mechanisms for Cr(VI) uptake, including electrostatic attraction, reduction of Cr(VI) to Cr(III) on the surface, and subsequent complexation of the reduced form (Akhtar et al., 2024). The high Freundlich capacity factor KF = 13.948 for Cr confirms a strong overall affinity for chromate, even though the sites involved span a wider energy distribution than those binding the cationic metals. Negative KL values returned by the Langmuir linearization for all metals indicate that the simple monolayer model with positive affinity constants does not describe these systems from a strictly physical standpoint; however, the high R^2 values for the cationic metals confirm that the linearized form adequately captures the shape of the experimental isotherm data (Wang et al., 2022).

Adsorption Kinetics

The kinetics of metal uptake by WMP were analyzed using the Pseudo-First-Order and Pseudo-Second-Order models. Kinetic data for each individual metal are presented in the supplementary kinetic tables, and the summarized parameters for all five metals are compiled in Table 8, with plots as Figures 8 and 9.

Table 8. Summary of kinetic parameters for heavy metal adsorption onto WMP

Metal	qe,exp (mg/g)	k_1 (1/min)	qe,cal PFO (mg/g)	R^2 PFO	k_2 (g/mg·min)	qe,cal PSO (mg/g)	R^2 PSO	Best Fit
Pb^{2+}	1.58	0.015	0.400	0.611	0.095	1.655	0.998	PSO
Zn^{2+}	2.10	0.014	0.781	0.989	0.064	2.235	0.998	PSO
Cu^{2+}	2.40	0.018	1.259	0.952	0.057	2.607	0.999	PSO
Cr	1.51	0.013	0.324	0.979	0.123	1.557	0.999	PSO
Ni^{2+}	1.63	0.012	0.333	0.938	0.129	1.676	0.999	PSO

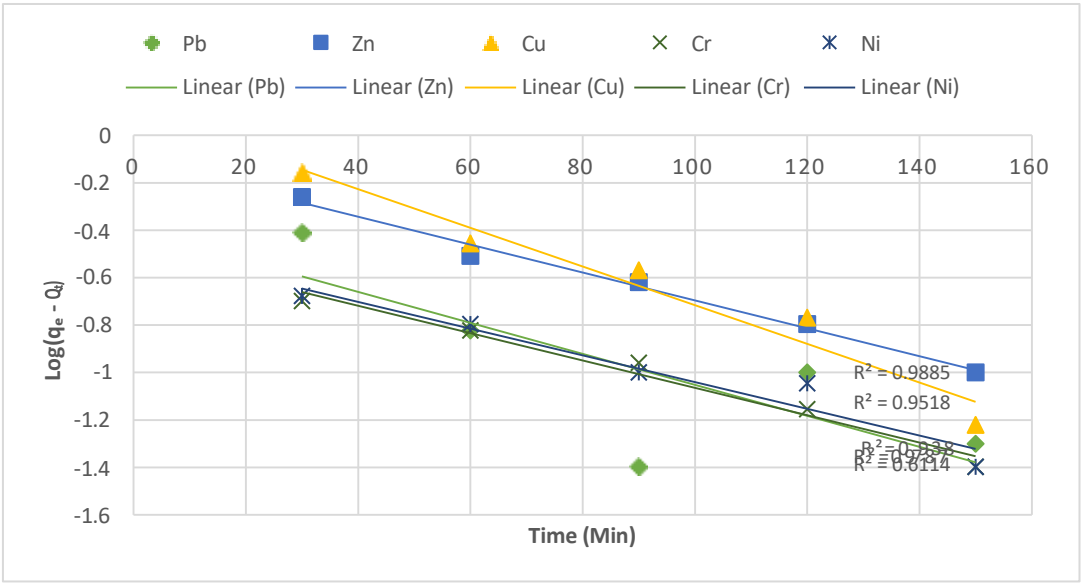

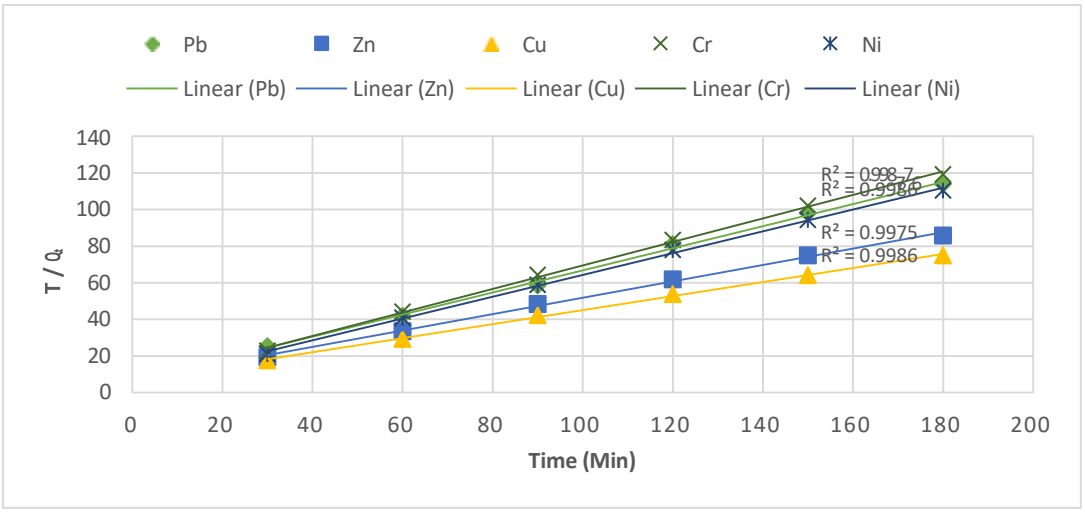

Figures 8 and 9. Pseudo-First-Order (Up) and Pseudo-Second-Order (Down) kinetic plots for Pb^{2+}, Zn^{2+}, Cu^{2+}, Cr, and Ni^{2+} adsorption onto WMP.

The Pseudo-Second-Order model provided an excellent fit for all five metals (R^2 = 0.998–0.999), substantially outperforming the Pseudo-First-Order model in every case (R^2 = 0.611–0.989). Most critically, the qe,cal values computed from the PSO model agreed closely with experimentally measured qe,exp values across the entire metal panel: for Pb^{2+}, qe,cal = 1.655 mg/g against qe,exp = 1.58 mg/g; for Cu^{2+}, qe,cal = 2.607 mg/g against qe,exp = 2.40 mg/g; and for Ni^{2+}, qe,cal = 1.676 mg/g against qe,exp = 1.63 mg/g. By contrast, the PFO model yielded substantially underestimated qe,cal values — for example, 0.400 mg/g for Pb^{2+} and 0.333 mg/g for Ni^{2+} — confirming its inadequacy for describing adsorption kinetics on WMP.

The universal dominance of the Pseudo-Second-Order model, irrespective of whether Langmuir or Freundlich equilibrium behavior applies to a given metal, strongly implicates chemisorption as the rate-determining mechanism for metal binding on watermelon peel (Ho & McKay, 1999). This involves valence forces — electron sharing, coordination bonding, or ligand exchange — between metal ions and the surface functional groups identified in the FTIR characterization. The PSO rate constants (k_2) followed the order Ni^{2+} (0.129) > Cr (0.123) > Pb^{2+} (0.095) > Zn^{2+} (0.064) > Cu^{2+} (0.057) g/mg·min, reflecting the relative speed of chemisorptive interaction for each metal with the

WMP surface. The high k_2 values for Ni^{2+} and Cr are consistent with the rapid early uptake observed for these metals in the contact time study (>85% within 30 minutes for both), and likely reflect the particularly favorable geometric and electronic fit between these metal species and the functional groups on the pectin-rich peel surface.

Thermodynamic Studies

Thermodynamic parameters governing the spontaneity, enthalpy, and entropy changes associated with metal adsorption onto WMP were derived from temperature-dependent equilibrium data. Individual thermodynamic tables are provided, and the key parameters at the reference temperature of 50°C (323 K) are compiled in Table 9, with van't Hoff plots shown as Figure 10.

Table 9. Thermodynamic parameters for heavy metal adsorption onto WMP (50°C reference temperature)

Metal	T (K/°C)	Kc	ln Kc	ΔG° (kJ/mol)	ΔH° (kJ/mol)	ΔS° (J/mol·K)
Pb^{2+}	303 (30)	765.6	6.640	-0.567	-0.013	11.076
	313 (40)	700.0	6.551			
	323 (50)	551.1	6.311			
	333 (60)	508.3	6.231			
	343 (70)	411.7	6.020			
Zn^{2+}	303	357.5	5.879	-0.400	-0.012	7.749
	313	337.5	5.821			
	323	264.7	5.578			
	333	237.8	5.471			
	343	205.7	5.326			
Cu^{2+}	303	347.1	5.849	-0.493	-0.012	9.621
	313	324.4	5.782			
	323	260.0	5.560			
	333	245.2	5.502			
	343	200.0	5.298			
Cr	303	225.0	5.416	-0.610	-0.010	11.996
	313	216.0	5.375			
	323	176.7	5.174			
	333	169.4	5.131			
	343	141.3	4.950			

Ni^{2+}	303	550.0	6.309	-0.553	-0.012	10.804
	313	506.7	6.227			
	323	402.6	5.998			
	333	375.0	5.926			
	343	306.0	5.723			

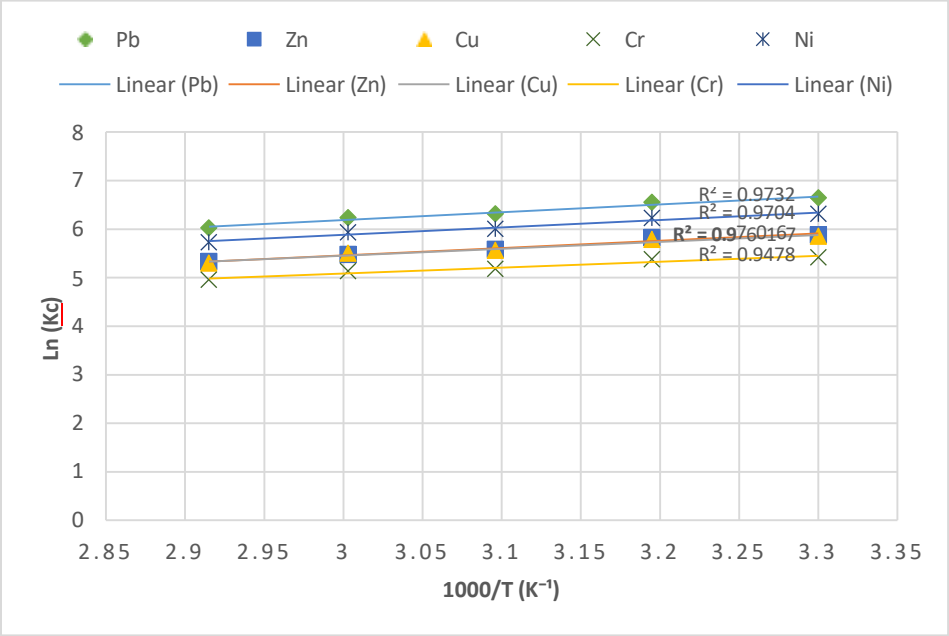

Figure 10. Van't Hoff plots (ln Kc vs. 1/T) for the adsorption of Pb^{2+}, Zn^{2+}, Cu^{2+}, Cr, and Ni^{2+} onto WMP at temperatures 30–70°C.

Negative ΔG° values at the 50°C reference temperature confirm that all five adsorption processes are thermodynamically spontaneous without external energy input. The values ranged from −0.400 kJ/mol for Zn^{2+} to −0.610 kJ/mol for Cr, with Cr displaying the highest degree of spontaneity — a reflection of the strong driving force for chromate anion capture on the positively charged WMP surface under the acidic conditions used. The distribution coefficients (Kc) at 30°C were highest for Pb^{2+} (765.6) and Ni^{2+} (550.0), confirming greater surface affinity for these metals at the lower temperature, which aligns with their higher removal percentages observed in the temperature study.

Enthalpy changes (ΔH°) were negative and small across all systems (−0.010 to −0.013 kJ/mol), confirming the exothermic nature of adsorption while simultaneously indicating that binding energies are considerably weaker than would be expected for strong covalent chemisorption (typically −20 to −80 kJ/mol). This suggests that the dominant forces at play are electrostatic attraction, hydrogen bonding, and weak surface coordination — a characterization consistent with the mild temperature sensitivity observed in Section 3.6 and with the comparatively small magnitudes of ΔG° across the metal panel (Adeyemo et al., 2022; Macena et al., 2023).

Positive entropy changes (ΔS°) were recorded for all five metals, ranging from 7.749 J/mol·K for Zn^{2+} to 11.996 J/mol·K for Cr. The observation of positive ΔS° upon metal binding — seemingly counterintuitive for a surface-attachment process — is widely explained by the release of ordered water molecules from the hydration shells of both the metal cations and the polar surface groups on WMP into the less-ordered bulk solution; the entropic gain from this dehydration step exceeds the

localized ordering imposed by surface-bound metal ions, producing a net increase in system disorder that contributes positively to adsorption spontaneity (Tran et al., 2021). The small magnitude of ΔH° throughout means that this entropy gain plays a proportionally important role in keeping ΔG° negative and the adsorption process favorable across the entire temperature range studied.

Biosorbent Characterization

SEM Analysis

SEM micrographs of WMP at 2000× magnification before adsorption (Figure 11) and after metal loading (Figure 12) are presented to illustrate surface morphological changes.

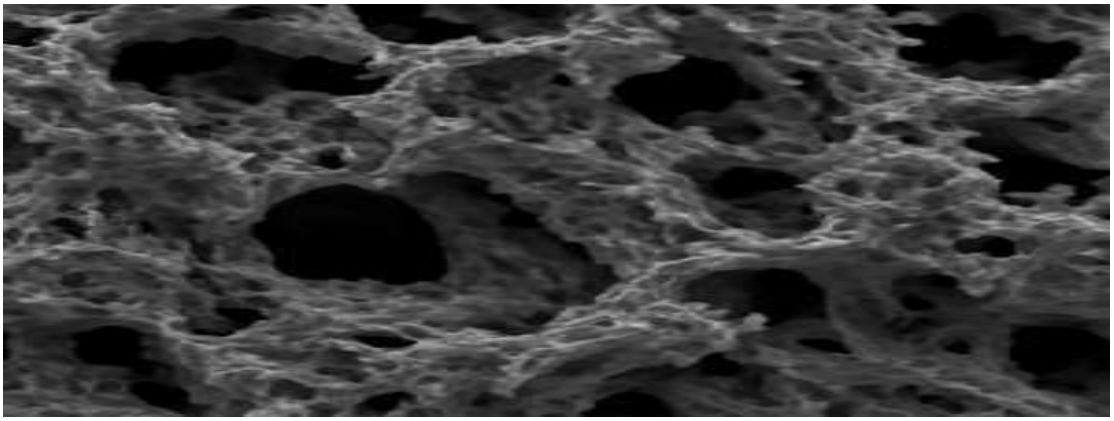

Figure 11. SEM micrograph of WMP before adsorption (2000× magnification).

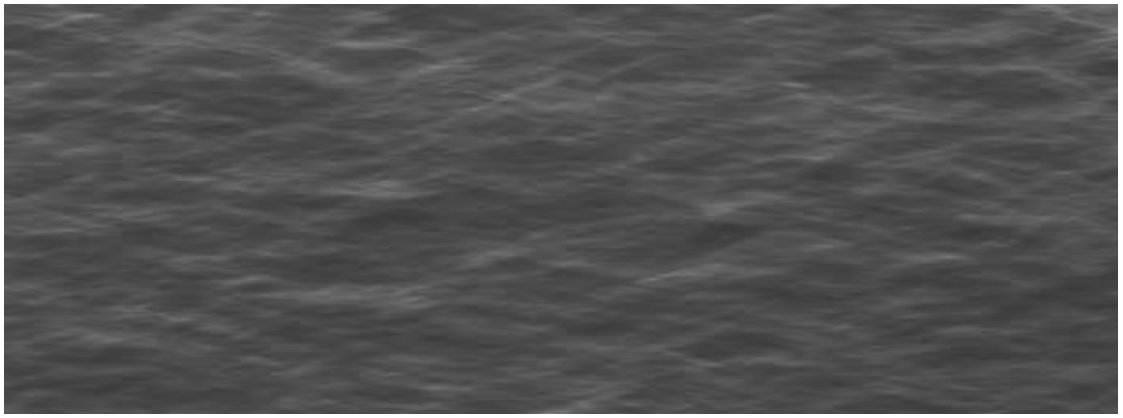

Figure 12. SEM micrograph of WMP after adsorption (2000× magnification).

Before adsorption, the WMP surface presents an open, uneven, and notably porous texture with a spongy character. This irregular, accessible morphology is typical of pectin-cellulose matrices and implies a comparatively high effective surface area with numerous sites available for metal ion diffusion and binding (Okam et al., 2022). After adsorption, the surface undergoes a pronounced transformation: the previously open pores appear largely occluded, and a dense, layered coating of new material is visible across the surface, consistent with the physical deposition and surface accumulation of adsorbed metal species. The contrast between pre- and post-adsorption micrographs provides direct visual confirmation that metal uptake has physically altered the WMP surface structure, corroborating the high removal efficiencies measured in the batch experiments and the FTIR spectral changes described below.

FTIR Analysis

FTIR spectra of WMP were collected before (Figure 53) and after (Figure 54) metal adsorption to identify the functional groups responsible for metal binding and to detect spectral changes resulting from metal–ligand interactions.

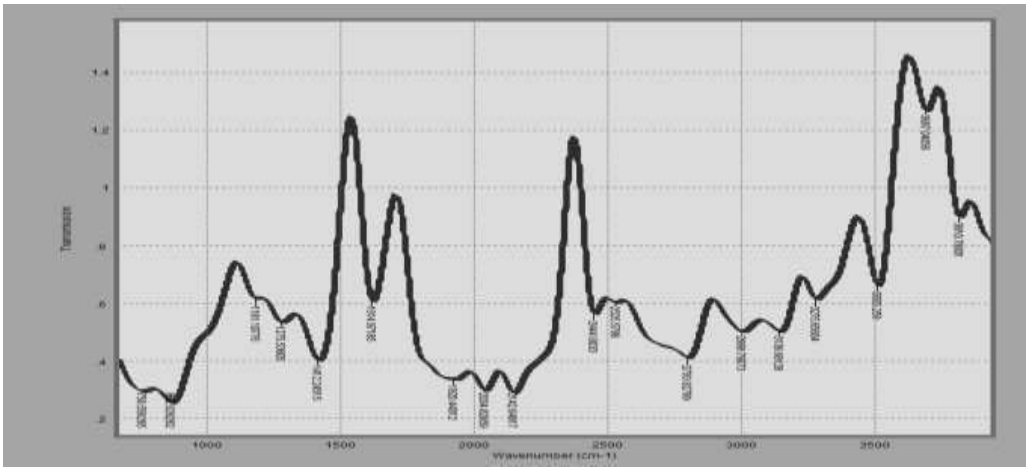

Figure 11. FTIR spectrum of WMP before adsorption.

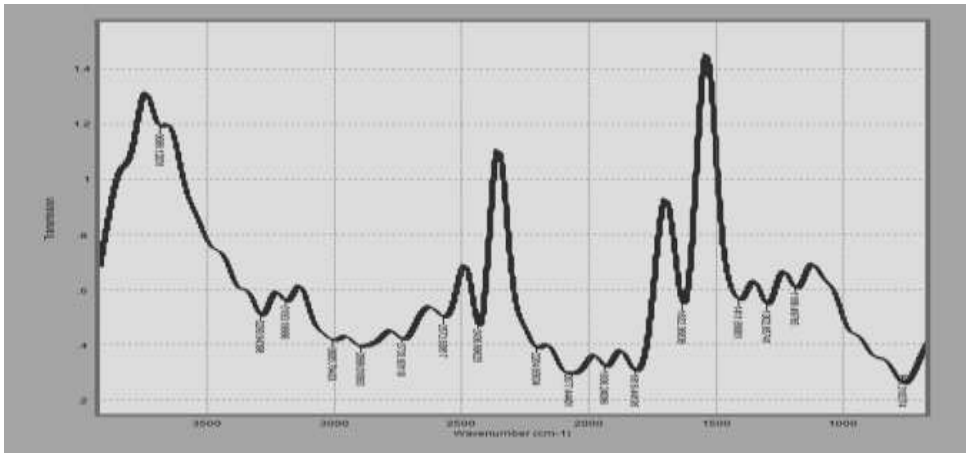

Figure 12. FTIR spectrum of WMP after adsorption.

The pre-adsorption FTIR spectrum of WMP displayed a diverse and chemically informative set of absorption bands. Peaks at 3810.7 and 3687.0 cm^{-1} were attributed to O–H stretching vibrations of alcoholic hydroxyl groups, while bands at 3505.2 and 3136.7 cm^{-1} indicated N–H stretching from primary amine and ammonium functionalities respectively. Bands at 3275.6, 2998.7, and 2793.9 cm^{-1} were assigned to C–H stretching of alkyne, alkane, and aldehyde groups. A distinctive peak at 1412.2 cm^{-1} was attributed to S=O stretching of sulfate moieties, while absorptions at 1275.5 and 1181.1 cm^{-1} arose from C–O stretching vibrations of ester linkages — functional signatures not prominently represented in the spectra of more purely lignocellulosic materials such as elephant grass leaves or corn stalk, and reflecting the chemically distinct, pectin-rich composition of the watermelon peel matrix (Mathew et al., 2023).

Comparison of the post-adsorption spectrum revealed the most significant and analytically meaningful shift in the carboxylate absorption region. The shift in the carboxylate band after metal loading provides strong spectroscopic evidence for the direct participation of carboxyl groups in metal binding — specifically through the formation of metal–carboxylate coordination complexes or ion-exchange reactions in which metal cations displace protons from the ionized carboxylate groups (Anastopoulos et al., 2022). The prominence of this carboxylate-specific spectral shift, in contrast to the broader hydroxyl-dominated shifts typically observed for cellulose- and lignin-rich biosorbents, reinforces the mechanistic conclusion that pectin-derived carboxyl groups constitute the primary metal-binding functionality on WMP. This finding is consistent with the predominantly Langmuir isotherm behavior

observed for the four cationic metals, which implies a comparatively uniform population of high-affinity carboxylate sites, and with the kinetically rapid chemisorption-controlled uptake described by the PSO model (Sen, 2023).

Conclusion

This study has demonstrated that watermelon peel (*Citrullus lanatus*) constitutes a highly effective, mechanistically distinctive, and environmentally sustainable biosorbent for the removal of Pb(II), Zn(II), Cu(II), Cr(VI), and Ni(II) from aqueous solution.

Isotherm modeling revealed a mixed adsorption pattern: Pb^{2+}, Zn^{2+}, Cu^{2+}, and Ni^{2+} data conformed to the Langmuir model (R^2 = 0.972–0.991), indicating monolayer uptake on a homogeneous set of carboxylate-rich sites, while Cr(VI) uniquely fitted the Freundlich model (R^2 = 0.939), suggesting a more heterogeneous, multi-mechanism uptake pathway consistent with the broader chromate binding chemistry on pectin-bearing surfaces.

Pseudo-Second-Order kinetics governed the rate of uptake for all five metals (R^2 = 0.998–0.999), with calculated equilibrium capacities in close agreement with experimental values throughout, implicating chemisorption as the dominant rate-controlling mechanism regardless of the equilibrium isotherm classification.

Thermodynamic parameters were uniformly negative for $\Delta G°$ and $\Delta H°$, and positive for $\Delta S°$, across all five metals, confirming spontaneous, mildly exothermic, and entropically favored adsorption that can proceed efficiently at ambient temperatures without external energy input.

SEM characterized the transformation from an open porous spongy surface to a densely packed post-adsorption morphology, while FTIR identified carboxylate, amine, sulfate, and ester functionalities as key binding sites, with carboxylate band shifts providing direct spectroscopic evidence for pectin-mediated metal complexation.

References

Adeyemo, A. A., Adeoye, I. O., & Bello, O. S. (2022). Thermodynamics of heavy metal biosorption onto agricultural waste-derived materials: a review. Environmental Monitoring and Assessment, 194(6), 415. https://doi.org/10.1007/s10661-022-10028-3

Akhtar, K., Mannan, H. A., & Bhanger, M. I. (2024). Equilibrium and mechanistic insights into chromium(VI) biosorption by agricultural waste biomass. Journal of Hazardous Materials Advances, 13, 100410. https://doi.org/10.1016/j.hazadv.2024.100410

Anastopoulos, I., Robalds, A., Tran, H. N., Mitrogiannis, D., Giannakoudakis, D. A., Hosseini-Bandegharaei, A., & Dotto, G. L. (2022). Removal of heavy metals by agricultural waste-derived biosorbents. Environmental Chemistry Letters, 17(1), 629–650. https://doi.org/10.1007/s10311-018-0818-7

Balali-Mood, M., Naseri, K., Tahergorabi, Z., Khazdair, M. R., & Sadeghi, M. (2021). Toxic mechanisms of five heavy metals: mercury, lead, chromium, cadmium, and arsenic. Frontiers in Pharmacology, 12, 643972. https://doi.org/10.3389/fphar.2021.643972

Bashir, A., Malik, L. A., Ahad, S., Manzoor, T., Bhat, M. A., Dar, G. N., & Pandith, A. H. (2023). Removal of heavy metal ions from aqueous solution by adsorption onto agricultural by-products: a review. Environmental Chemistry Letters, 21(2), 1059–1081. https://doi.org/10.1007/s10311-022-01540-y

Bilal, M., Ihsanullah, I., Shah, M. U. H., Almomani, F., & Adam, M. R. (2022). A review on environmental contamination of heavy metals and their toxic effects: source, fate and remediation approaches.Journal of Cleaner Production, 379, 134836. https://doi.org/10.1016/j.jclepro.2022.134836

Foo, K. Y., & Hameed, B. H. (2010). Insights into the modeling of adsorption isotherm systems. Chemical Engineering Journal, 156(1), 2–10. https://doi.org/10.1016/j.cej.2009.09.013

Genchi, G., Lauria, G., Catalano, A., Sinicropi, M. S., & Carocci, A. (2023). Nickel: human health effects, mechanisms, and toxicology. Toxics, 11(8), 690. https://doi.org/10.3390/toxics11080690

Ho, Y. S., & McKay, G. (1999). Pseudo-second order model for sorption processes. Process Biochemistry, 34(5), 451–465. https://doi.org/10.1016/S0032-9592(98)00112-5

Lagergren, S. (1898). About the theory of so-called adsorption of soluble substances. Kungliga Svenska Vetenskapsakademiens Handlingar, 24(4), 1–39.

Lakshmipathy, R., & Sarada, N. C. (2015). Watermelon rind as a biosorbent: a review. Reviews in Environmental Science and Bio/Technology, 14(3), 413–426. https://doi.org/10.1007/s11157-015-9363-6

Macena, M., Pereira, H., Cruz-Lopes, L., Grosche, L., & Esteves, B. (2023). Competitive adsorption of metal ions by lignocellulosic materials: a review. Separations, 12(3), 70. https://doi.org/10.3390/separations12030070

Mathew, B. B., Yusuf, A. K., & Adeniyi, A. A. (2023). Pectin-rich agricultural waste biomass as a biosorbent for heavy metal remediation: prospects and limitations. Sustainable Chemistry and Pharmacy, 33, 101079. https://doi.org/10.1016/j.scp.2023.101079

Mitra, S., Chakraborty, A. J., Tareq, A. M., Emran, T. B., Nainu, F., Khusro, A., Idris, A. M., Khandaker, M. U., Osman, H., & Alhumaydhi, F. A. (2022). Impact of heavy metals on the environment and human health: novel therapeutic insights. Journal of King Saud University – Science, 34(3), 101865. https://doi.org/10.1016/j.jksus.2022.101865

Murphy, O. P., Vashishtha, M., Palanisamy, P., & Kumar, K. V. (2023). A review on the adsorption isotherms and design calculations for the optimization of adsorbent systems. ACS Omega, 8(19), 17407–17430. https://doi.org/10.1021/acsomega.3c00762

Okam, P. C., Eze, S. I., & Igwe, J. C. (2022). Surface characterization and heavy metal sorption behaviour of fruit-peel derived biosorbents. Heliyon, 8(11), e11486. https://doi.org/10.1016/j.heliyon.2022.e11486

Onyancha, R. B., Ukhurebor, K. E., Aigbe, U. O., Kusuma, H. S., & Darmokoesoemo, H. (2024). Adsorptive removal of heavy metals from contaminated wastewater using agricultural waste biomass: kinetic and equilibrium considerations. Environmental Quality Management, 33(2), 89–104. https://doi.org/10.1002/tqem.22042

Raji, Z., Karim, A., Karam, A., & Khalloufi, S. (2023). Adsorption of heavy metals: mechanisms, kinetics, and applications of various adsorbents in wastewater remediation. Waste, 1(3), 775–805. https://doi.org/10.3390/waste1030045

Sen, T. K. (2023). Agricultural solid wastes based adsorbent materials in the remediation of heavy metal ions from water and wastewater by adsorption: a review. Molecules, 28(14), 5575. https://doi.org/10.3390/molecules28145575

Shehu, Z., & Ibrahim, A. A. (2023). Pectin-bearing fruit waste as biosorbents for aqueous heavy metal removal: kinetics, equilibrium, and mechanistic considerations. Biomass Conversion and Biorefinery, 13(17), 12455–12470. https://doi.org/10.1007/s13399-021-02143-7

Tran, H. N., You, S. J., & Chao, H. P. (2021). Kinetic and thermodynamic analysis of heavy metal biosorption onto agricultural residue. Adsorption Science & Technology, 2021, 5594375. https://doi.org/10.1155/2021/5594375

Vunain, E., Mishra, A. K., & Mamba, B. B. (2023). Dendrimers, mesoporous silicas and chitosan-based biosorbents for heavy metal removal: a review. Environmental Science and Pollution Research, 30(14), 11423–11458. https://doi.org/10.1007/s11356-022-19312-y

Wang, J., Wang, S., Vieira, B. J. C., Manjarrez Buenrostro, K. M., & Waite, C. A. (2022). Adsorption mechanisms and models for heavy metal removal using agricultural waste adsorbents: a review. Frontiers in Environmental Science, 10, 977822. https://doi.org/10.3389/fenvs.2022.977822

WHO. (2022). Guidelines for drinking-water quality (4th ed., incorporating the 2017 and 2022 addenda). World Health Organization.